IOP Publishing Smart Materials and Structures
Smart Mater. Struct. 30 (2021) 045008 (14pp) https://doi.org/10.1088/1361-665X/abe033

An SECE array of piezoelectric energy harvesting

P H Wu, J T Lin, Y C Lo and Y C Shu*

Institute of Applied Mechanics, National Taiwan University, Taipei 106, Taiwan, Republic of China

E-mail: yichung@iam.ntu.edu.tw

Received 14 December 2020, revised 14 January 2021
Accepted for publication 26 January 2021
Published 25 February 2021

Abstract

The paper studies the electrical response of an array of piezoelectric oscillators attached to the synchronized electric charge extraction (SECE) interface circuit. The analytic estimate of output power is derived and presented through the matrix formulation of generalized Ohm's law (charging on capacitance) for the case of parallel (series) connection of energy harvesters. These formulations mainly depend on the proposed equivalent load impedances which are independent of external resistive loads. It therefore offers an advantage of enabling harvested power independent of DC output voltage and making the harvester array desirable for broadband energy scavenging. The proposed framework is subsequently validated both numerically and experimentally. The results show that the power output and bandwidth of an SECE-based array are superior to that based on the standard energy harvesting circuit. Further, it is found that the behavior of an SECE array electrically arranged in parallel connection is different from that connected in series. The former demonstrates the output power higher than the latter, while the latter exhibits roughly uniform peak power in frequency response. However, the experiment indicates the unexpected power drop deviated significantly from the prediction in the array of harvesters connected in series. Such a discrepancy is explained as a result of comparatively serious leakage current in the reverse-biased diodes.

Keywords: array of piezoelectric oscillators, equivalent load impedance, parallel/series connection of harvesters, piezoelectric energy harvesting, SECE interface circuit

1. Introduction

Energy harvesting from environmental sources has the potential to power remote wireless sensors which originally rely on batteries for power supply. But chemical batteries are toxic to the environment and need constant replacement which is tedious and expensive for the widely spread of sensors. This motivates the significant growth of vibration-based energy harvesting because of the ubiquitous presence of ambient vibrations. Among various transducers used in this technology [1–3], piezoelectric transduction is widely adopted due to various advantages [4]. These include the features of high electromechanical coupling, high voltage causing convenient design of power conditioning circuits, and the easy implementation in microsystems [5, 6]. Hence, piezoelectric energy harvesting has received huge attention from worldwide research efforts for decades. Advances enhancing such technology are numerous from many aspects, including mechanical structures [7–12], materials [13], and circuits [14–20]. In addition, there is a significant rise in the system-level designs based on the finite element methods coupled with several circuit solvers in the past years [21–25].

But the majority of these works were based on resonant vibration of a single piezoelectric oscillator for harvesting energy. The consequence of it is the huge amount of power reduction observed at around off-resonance in these devices. It therefore motivates extensive research efforts on improving such technology. These include changing mechanical or electric configurations for resonant tuning [26–28], employing non-linearity for enlarging operational bandwidth [29–31], or using the frequency up-conversion transforming the low frequency of plucking into the high frequency of resonant vibration [32–34]. Another popular method is to develop harvester

* Author to whom any correspondence should be addressed.

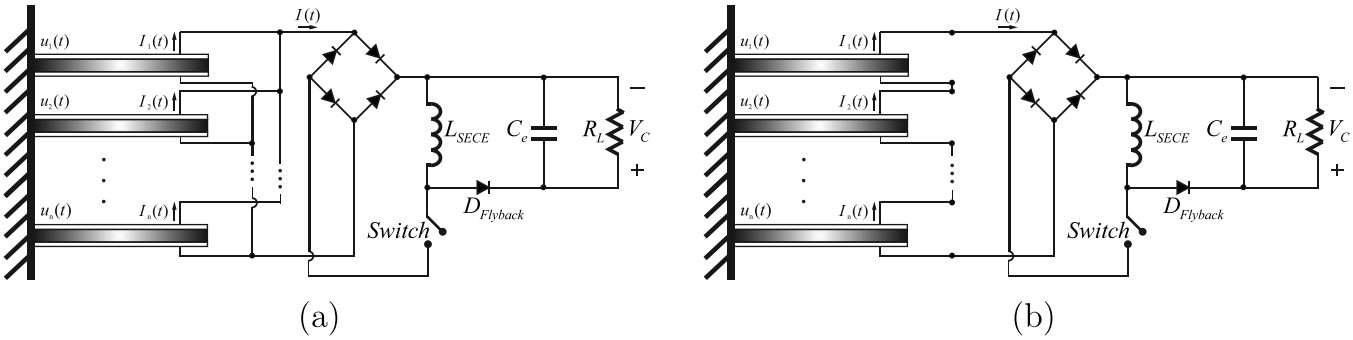

Figure 1. An array of multiple piezoelectric oscillators attached to an SECE interface circuit: (a) parallel connection and (b) series connection.

arrays for improving bandwidth and enhancing power output. Its operational principle is simple enough for covering the frequency range of excitation by adjusting the resonant frequency of each oscillator [35–37]. Thus, various forms of harvester arrays were developed for serving specific applications, including the configurations of cantilever [38, 39], Z-type beam [40], fan-structure [41], circular diaphragm [42] and MEMS [43]. In spite of these activities developed for broadband energy harvesting, little had paid attention to the inclusion of the power conditioning circuits in these array works [44–46]. Instead, Lien and Shu [36] and Lin *et al* [47] had taken into account several energy harvesting circuits such as the standard (STD) and the synchronized switch harvesting on inductor (SSHI) interfaces in the cases of the parallel and series connection of piezoelectric oscillators, respectively. But a drawback of them was that the peak power driven at around the resonance of each harvester was not uniform within the frequency range of consideration. Such a defect has been recently resolved by Wu *et al* [48] considering the integration of multiple piezoelectric oscillators with mixed parallel-series connection.

This paper investigates the electrical response of the piezoelectric harvester array endowed with the synchronized electric charge extraction (SECE) interface circuit. Notice that the power conditioning circuits implemented in the aforementioned harvester arrays are load dependent and therefore, additional circuit modules such as DC–DC converters are required for insuring impedance matching under load variations. But the SECE interface enjoys the unique feature of load independence and is capable of enhancing power output in the case of weak/mild electromechanical coupling [49]. Thus, the harvester array attached to this circuit has the potential of being operated under irregular excitations [50]. Indeed, the SECE circuit was originally developed by Lefeuvre *et al* [51]. However, the requirement of precise control of switching time for maximum power output makes the SECE circuit difficult to be operated and self-powered. Thus, there were numerous works for improving this circuit technology, such as the OSECE (optimized SECE) and SP-OSECE (self-powered OSECE) proposed for simplifying the control strategy [52, 53]. Other variants of SECE were subsequently proposed for performance improvements at many aspects. These include (a) the tunable SECE [54], N-SECE [55] and SECPE (synchronous electric charge partial extraction) proposed for highly coupled piezoelectric energy scavengers [56]; (b) the PS-SECE (phase-shifted SECE) [57] and FT-SECE (frequency-tuning SECE) proposed for bandwidth improvement; [58] (c) the C-SP-SECE (compact self-powered SECE) [59, 60] and SP-ESECE (self-powered efficient SECE) [61] proposed for ameliorating the self-powered circuit performance; (d) the combination of SECE and the synchronized voltage inversion for power enhancement [62–64]. In addition, the SECE technique has been applied to non-linear energy harvesters [65–67], multi-sources [68–71] and wind energy harvesting [72].

The paper is organized as follows. The model development of an SECE-based array of piezoelectric oscillators is presented in section 2. The SECE output power is analytically derived and explicitly expressed for parallel and series connection patterns. The results are numerically validated in section 3 and experimentally justified in section 4. The conclusions are made in section 5.

2. Framework

An array of piezoelectric harvesters is considered and arranged electrically either in parallel or in series, as demonstrated in figure 1. Here the deviations in the parameters of each piezoelectric harvester are assumed to be small. The modal density of each generator is also assumed to be widely separated as in the case of cantilever configuration. Thus, if the whole device is excited at around its resonant frequency, the parameter model of this harvester array can be described by [36, 47]:

$$M_n\ddot{u}_n(t) + \eta_n\dot{u}_n(t) + K_n u_n(t) + \Theta_n V_{p_n}(t) = F_n(t), \quad (1)$$

$$-\Theta_n\dot{u}_n(t) + C_{p_n}\dot{V}_{p_n}(t) = -I_n(t), \quad (2)$$

where $n = 1, 2, \ldots, N$, N is the total number of oscillators, u_n the displacement of the nth mass M_n, V_{p_n} the voltage across the nth piezoelectric element, and $I_n(t)$ the current flowing into the specified circuit. In addition, above η_n, K_n, Θ_n and C_{p_n} are the mechanical damping coefficient, the stiffness, the piezoelectric coefficient and the capacitance of the nth piezoelectric oscillator. Below, the applied force $F_n(t)$ exerted to the

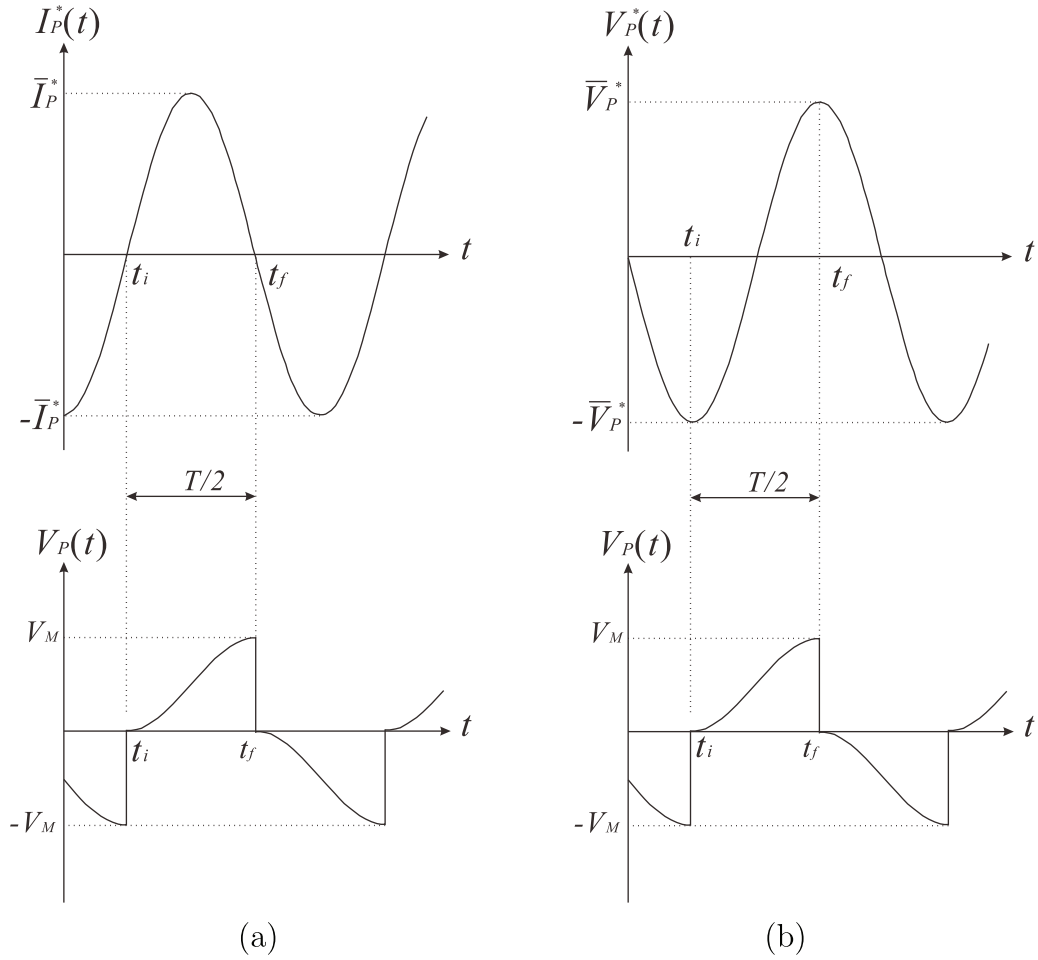

Figure 2. (a). Typical waveforms of the overall equivalent velocity current $I_p^*(t)$ and the piezoelectric voltage $V_p(t)$ in the case of parallel connection. (b) Typical waveforms of the overall equivalent displacement voltage $V_p^*(t)$ and the piezoelectric voltage $V_p(t)$ in the case of series connection.

nth harvester is assumed to be harmonic of a single signal of the form:

$$F_n(t) = \bar{F}_n \cos wt, \tag{3}$$

where $\bar{F}_n$ is the magnitude and w is the angular frequency in radians per second.

The harvester array is attached to an SECE interface circuit as also shown in figure 1. Different from the standard (STD) interface circuit consisting of an AC–DC full-bridge rectifier followed by a filtering capacitance C_e for smoothing the DC voltage V_c across the load R_L, the SECE interface circuit includes an inductor L_{SECE}, a switch, and a flyback diode D_{Flyback}. The working principle of this SECE circuit will be described separately for different electric connections of oscillators in the subsequent sections. Before doing that, notice that in writing equation (3) the array is assumed to be placed on a single excitation source. However, if harvesters are located at different places whose excitation frequencies are widely separated, the proposed setup is not appropriate. Under this circumstance, the respective electric rectification by employing multiple diodes might be suitable for avoiding charge cancelation [70, 73].

2.1. Parallel connection

Suppose all the oscillators are connected in parallel, as shown in figure 1(a). This gives,

$$V_p = V_{p_n}, \quad I(t) = \sum_{n=1}^{N} I_n(t), \tag{4}$$

where $V_p(t)$ and $I(t)$ are the alternating piezoelectric voltage and the overall current flowing into the specified circuit. It follows that equation (2) can be rewritten as:

$$I_p^*(t) = C_p^* \dot{V}_p(t) + I(t), \tag{5}$$

where

$$I_{p_n}^*(t) = \Theta_n \dot{u}_n(t),\ I_p^*(t) = \sum_{n=1}^{N} I_{p_n}^*(t),\ C_p^* = \sum_{n=1}^{N} C_{p_n}. \tag{6}$$

Note that $I_{p_n}^*(t)$ is interpreted as the equivalent velocity current of the nth oscillator, $I_p^*(t)$ is viewed as the overall equivalent velocity current, and C_p^* is the overall piezoelectric

capacitance. Under the steady state operation, the displacement of each harvester takes the form of:

$$u_n(t) = \bar{u}_n \cos(wt - \theta_n), \tag{7}$$

where $\bar{u}_n$ is the magnitude of displacement and θ_n is the relative phase shift. Substituting equation (7) into equation (6) gives:

$$I_p^*(t) = \bar{I}_p^* \sin(wt - \theta), \tag{8}$$

where θ is the phase shift and $\bar{I}_p^*$ is the magnitude of $I_p^*(t)$ which is related to the magnitude of displacement $\bar{u}_n$ by [36]:

$$\bar{I}_p^* = -\sum_{n=1}^{N} w\Theta_n \bar{u}_n e^{j(\theta-\theta_n)}, \quad j^2 = -1. \tag{9}$$

The operation of an SECE circuit of the present case is described as follows. The switch illustrated in figure 1(a) is open for the majority of time during the excitation period. But it is triggered at the vanishing points of $I_p^*(t)$ and is closed for a very short time. As a result, the charge extraction is initiated by converting the electrostatic energy to magnetic energy by the fast *LC* circuit oscillation during the switching period. After the switch is reopened, the energy stored in the inductor L_{SECE} is transferred to the load resistance R_L through the flyback diode. The typical waveforms of $I_p^*(t)$ and $V_p(t)$, for instance, are schematically illustrated in figure 2(a) where V_M is the magnitude of piezoelectric voltage $V_p(t)$. Notice that the current $I(t) = 0$ when the switch is open. The vanishing of $I_p^*(t)$, from equation (5), results in $\dot{V}_p(t) = 0$. Thus, the criterion of switching is substituted by monitoring the extreme value of the piezoelectric voltage. Practically, a control circuit is required to be implemented for detecting the peak voltage [74].

Now let $T = \frac{2\pi}{w}$ denote the period of mechanical excitation and t_i and t_f be two time instants such that $t_f - t_i = \frac{T}{2}$ and they correspond to $I_p^*(t_i) = I_p^*(t_f) = 0$, as demonstrated by figure 2(a). As the switch is off within the time period (t_i^+, t_f^-), this gives the current $I(t) = 0$ under the open circuit excitation. Thus, the principle of balance of charge conservation given by equation (5) provides:

$$\int_{t_i^+}^{t_f^-} I_p^*(t)\mathrm{d}t = \int_{t_i^+}^{t_f^-} \left(C_p^* \dot{V}_p(t) + I(t)\right)\mathrm{d}t = \int_{t_i^+}^{t_f^-} C_p^* \dot{V}_p(t)\mathrm{d}t. \tag{10}$$

Substituting the expression of $I_p^*(t) = \bar{I}_p^* \sin(wt - \theta)$ as in equation (8) into equation (10) gives:

$$V_M = \frac{2}{wC_p^*}\bar{I}_p^*. \tag{11}$$

Note that in deriving equation (11), for instance, it is set $t_i = \frac{\theta}{w}$ and $t_f = \frac{\pi+\theta}{w}$ which corresponds to $V_p(t_i^+) = 0$ and $V_p(t_f^-) = V_M$, as illustrated by figure 2(a).

The next step is the consideration of the balance of generalized energy. Indeed, the multiplication of $I_p^*(t)$ by equation (1) and the multiplication of $V_p(t)$ by equation (5) gives:

$$\begin{aligned}&\int_{t_i^+}^{t_f^-} \{M_n\ddot{u}_n(t) + \eta_n\dot{u}_n(t) + K_n u_n(t)\} I_p^*(t)\mathrm{d}t \\ &+ \int_{t_i^+}^{t_f^-} \left\{\Theta_n C_p^* V_p(t)\dot{V}_p(t) + \Theta_n V_p(t) I(t)\right\}\mathrm{d}t \\ &= \int_{t_i^+}^{t_f^-} I_p^*(t) F_n(t)\mathrm{d}t.\end{aligned} \tag{12}$$

Substituting equations (7) and (8) into equation (12) results in:

$$\begin{aligned}&\left(\frac{\pi}{2}wM_n \sin(\theta-\theta_n) - \frac{\pi}{2}\eta_n \cos(\theta-\theta_n)\right. \\ &\left. - \frac{\pi}{2w}K_n \sin(\theta-\theta_n)\right)\bar{I}_p^*\bar{u}_n + \left(\frac{1}{2}C_p^*\Theta_n V_M^2 + 0\right) \\ &= -\frac{\pi}{2w}\bar{F}_n\bar{I}_p^* \sin\theta.\end{aligned} \tag{13}$$

Combining equations (11) and (13) gives:

$$\begin{aligned}&-(K_n - w^2M_n)\bar{u}_n \sin(\theta-\theta_n) - w\eta_n\bar{u}_n \cos(\theta-\theta_n) \\ &+ \frac{4\Theta_n}{w\pi C_p^*}\bar{I}_p^* = -\bar{F}_n \sin\theta.\end{aligned} \tag{14}$$

Note that $V_{p_n}(t)$ in equation (1) can be eliminated by equations (4) and (5) due to the parallel connection of oscillators. It gives,

$$\begin{aligned}&\int_{t_i^+}^{t_f^-} \left\{M_n\frac{d}{\mathrm{d}t}\ddot{u}_n(t) + \eta_n\frac{d}{\mathrm{d}t}\dot{u}_n(t) + K_n\frac{d}{\mathrm{d}t}u_n(t)\right. \\ &\left. + \frac{\Theta_n}{C_p^*}\left[I_p^*(t) - I(t)\right]\right\}\mathrm{d}t = \int_{t_i^+}^{t_f^-} \frac{d}{\mathrm{d}t}F_n(t)\mathrm{d}t,\end{aligned} \tag{15}$$

which in turn provides:

$$\begin{aligned}&-(K_n - w^2M_n)\bar{u}_n \cos(\theta-\theta_n) + w\eta_n\bar{u}_n \sin(\theta-\theta_n) \\ &+ \frac{\Theta_n}{wC_p^*}\bar{I}_p^* = -\bar{F}_n \cos\theta.\end{aligned} \tag{16}$$

The summation of equation (14) multiplied by an imaginary number j and equation (16) gives:

$$\begin{aligned}&-(K_n - w^2M_n)\bar{u}_n e^{j(\theta-\theta_n)} - jw\eta_n\bar{u}_n e^{j(\theta-\theta_n)} \\ &+ \frac{\Theta_n}{wC_p^*}\left(1 + j\frac{4}{\pi}\right)\bar{I}_p^* = -\bar{F}_n e^{j\theta}.\end{aligned}$$

The elimination of $e^{j\theta}$ on both sides of the above equation leads to:

$$\begin{aligned}&\frac{(K_n - w^2M_n)}{w\Theta_n^2}(w\Theta_n\bar{u}_n)e^{-j\theta_n} + j\frac{\eta_n}{\Theta_n^2}(w\Theta_n\bar{u}_n)e^{-j\theta_n} \\ &- \frac{1}{wC_p^*}\left(1 + j\frac{4}{\pi}\right)\bar{I}_p^* e^{-j\theta} = \frac{\bar{F}_n}{\Theta_n}.\end{aligned} \tag{17}$$

Finally, introduce:

$$\hat{V}_n = \frac{\bar{F}_n}{\Theta_n}, \quad \hat{I}_n = jw\Theta_n\bar{u}_n e^{-j\theta_n}, \quad n = 1,\ldots,N. \tag{18}$$

Recalling the expression of $\bar{I}_p^*$ by equation (9) gives:

$$\bar{I}_p^* e^{-j\theta} = j\sum_{k=1}^{N} jw\Theta_n\bar{u}_n e^{-j\theta_n} = j\sum_{k=1}^{N}\hat{I}_k.$$

The substitution of the above equation into equation (17) provides the matrix formulation of the generalized Ohm's law [75]:

$$\hat{\mathbf{V}} = \hat{\mathbf{Z}}\hat{\mathbf{I}}, \quad \hat{\mathbf{V}} = \left(\hat{V}_n\right), \quad \hat{\mathbf{I}} = \left(\hat{I}_n\right), \tag{19}$$

where $\hat{\mathbf{Z}}$ is the generalized impedance matrix given by:

$$\hat{Z}_{kl} = \begin{cases} \frac{\eta_k}{\Theta_k^2} + j\frac{wM_k}{\Theta_k^2} - j\frac{K_k}{w\Theta_k^2} + Z_{\text{eq}}^p & \text{if } k = l, \\ Z_{\text{eq}}^p & \text{if } k \neq l, \end{cases} \tag{20}$$

with the equivalence load impedance Z_{eq}^p defined by:

$$Z_{\text{eq}}^p = \frac{4}{\pi w C_p^*} - j\frac{1}{wC_p^*}. \tag{21}$$

The average harvested power during the half-period of vibration is therefore,

$$P_h = \frac{\frac{1}{2}C_p^* V_M^2}{\frac{T}{2}}, \quad V_M = \frac{2}{wC_p^*}\left|\sum_{n=1}^{N}\hat{I}_n\right|, \tag{22}$$

where the magnitude of piezoelectric voltage V_M is derived by equations (9), (11) and (18). Each $\hat{I}_n$ in equation (22) is acquired by the inversion of the matrix formulation of generalized Ohm's law defined by equation (19). Finally, a comment is made on the methodology of deriving the array solution. Tang and Yang [49] have derived an analytic estimate of power output for a single piezoelectric harvester attached to an SECE circuit. The main difference in methodology is that the overall equivalent velocity current, $I_p^*(t) = \sum_{n=1}^{N}\Theta_n\dot{u}_n(t)$ as in equation (6), is introduced in the balance of charge formulation as in equation (10), the balance of generalized energy as in equation (12) and in the replacement of $V_{p_n}(t)$ as in equation (15).

2.2. Series connection

Alternatively, suppose all the piezoelectric oscillators are serially connected as demonstrated in figure 1(b). This gives,

$$V_p(t) = \sum_{n=1}^{N} V_{p_n}(t), \quad I(t) = I_n(t), \tag{23}$$

where $V_p(t)$ is the overall piezoelectric voltage and $I(t)$ is the current flowing into the specified circuit. Thus, equation (2) can be rewritten as:

$$\dot{V}_p^*(t) = \dot{V}_p(t) + \frac{1}{C_p^*}I(t). \tag{24}$$

Above

$$V_{p_n}^*(t) = \frac{\Theta_n}{C_{p_n}}u_n(t), \quad V_p^*(t) = \sum_{n=1}^{N} V_{p_n}^*(t), \quad \frac{1}{C_p^*} = \sum_{n=1}^{N}\frac{1}{C_{p_n}}, \tag{25}$$

where $V_{p_n}^*(t)$ is interpreted as the equivalent displacement voltage of the nth oscillator, $V_p^*(t)$ is the overall equivalent displacement voltage, and C_p^* is the overall piezoelectric capacitance.

The displacement of each oscillator, under the steady state excitation, is set to be of the form described by equation (7). Thus, from equation (25), the overall equivalent displacement voltage due to vibration can be expressed as:

$$V_p^*(t) = \bar{V}_p^*\cos(wt - \theta), \tag{26}$$

where θ is the phase shift and $\bar{V}_p^*$ is the magnitude of $V_p^*(t)$. It can be shown that $\bar{V}_p^*$ is related to $\bar{u}_n$ by [47]:

$$\bar{V}_p^* = \sum_{n=1}^{N}\frac{\Theta_n}{C_{p_n}}\bar{u}_n e^{j(\theta-\theta_n)}. \tag{27}$$

The series connection of piezoelectric oscillators is attached to an SECE interface circuit as also shown in figure 1(b). The switch is open for the majority of time during excitation. But different from the previous case, it is triggered at the maximum/minimum points of $V_p^*(t)$ for a very short time. It results in the LC circuit oscillation so that energy of capacitance is transferred to L_{SECE} within the duration of switching. Then, similar to the previous case, the reopening of the switch allows the energy stored in L_{SECE} to the circuit output through the flyback diode. The typical waveforms of $V_p^*(t)$ and $V_p(t)$ are schematically demonstrated in figure 2(b) where V_M is the magnitude of piezoelectric voltage $V_p(t)$.

To derive an estimate of harvested power of the present case, consider the balance of charge first. Again let T denote the period of mechanical excitation and t_i and t_f be two time instants such that $V_p^*(t_i) = -\bar{V}_p^*$, $V_p^*(t_f) = \bar{V}_p^*$ and $t_f - t_i = \frac{T}{2}$, as demonstrated in figure 2(b). The consideration of equation (24) provides:

$$\int_{t_i^+}^{t_f^-}\dot{V}_p^*(t)\mathrm{d}t = \int_{t_i^+}^{t_f^-}\dot{V}_p(t)\mathrm{d}t, \tag{28}$$

since the switch is off within this period. It follows that:

$$2\bar{V}_p^* = V_M. \tag{29}$$

The next is to consider the balance of generalized energy. Different from the previous one, equation (1) is multiplied by $\dot{V}_p^*(t)$ rather than $I_p^*(t)$. In addition, V_{p_n} in equation (1) is eliminated using equation (2). Indeed, this gives:

$$\int_{t_i^+}^{t_f^-}\left(M_n\ddot{u}_n(t) + \eta_n\dot{u}_n(t) + K_n u_n(t) + \frac{\Theta_n^2}{C_{p_n}}u_n(t) + \frac{\Theta_n}{C_{p_n}}Q(t)\right)\dot{V}_p^*(t)\mathrm{d}t = \int_{t_i^+}^{t_f^-}F_n(t)\dot{V}_p^*(t)\mathrm{d}t, \tag{30}$$

where $I(t) = -\frac{d}{dt}Q(t)$ and $Q = Q_n$ due to the series connection of piezoelectric oscillators. Note that the use of equation (24) gives:

$$\begin{aligned}\frac{1}{C_p^*}\int_{t_i^+}^{t_f^-} \dot{V}_p^*(t)Q(t)\mathrm{d}t &= \int_{t_i^+}^{t_f^-} \dot{V}_p^*(t)V_p(t)\mathrm{d}t - \int_{t_i^+}^{t_f^-} \dot{V}_p^*(t)V_p^*(t)\mathrm{d}t \\ &= \int_{t_i^+}^{t_f^-} \left(\dot{V}_p(t) + \frac{1}{C_p^*}I_p(t)\right)V_p(t)\mathrm{d}t \\ &\quad - \frac{1}{2}\left[V_p^*(t)\right]^2\Big|_{t_i^+}^{t_f^-} \\ &= \frac{1}{2}\left[V_p(t)\right]^2\Big|_{t_i^+}^{t_f^-} - \frac{1}{2}\left[(\bar{V}_p^*)^2 - (-\bar{V}_p^*)^2\right] \\ &= \frac{1}{2}V_M^2 \\ &= 2\bar{V}_p^{*^2}, \end{aligned} \tag{31}$$

due to equation (29). Finally, substituting equations (7), (26) and (31) into equation (30) provides:

$$\left[\left(K_n - w^2M_n + \frac{\Theta_n^2}{C_{p_n}}\right)\sin(\theta-\theta_n) + w\eta_n\cos(\theta-\theta_n)\right]\bar{u}_n + \frac{4\Theta_n}{\pi C_{p_n}}C_p^*\bar{V}_p^* = \bar{F}_n\sin\theta. \tag{32}$$

The final step is to consider the balance of electromechanical dynamics. Indeed, equation (1) can be reformulated by eliminating $V_{p_n}(t)$ from equation (2). This provides,

$$M_n\frac{d}{dt}\ddot{u}_n(t) + \eta_n\frac{d}{dt}\dot{u}_n(t) + K_n\frac{d}{dt}u_n(t) + \frac{\Theta_n^2}{C_{p_n}}\frac{d}{dt}u_n(t) - \frac{\Theta_n}{C_{p_n}}I(t) = \frac{d}{dt}F_n(t). \tag{33}$$

The integration of equation (33) over the half cycle from t_i^+ to t_f^- using equation (7) provides:

$$\left[\left(K_n - w^2M_n + \frac{\Theta_n^2}{C_{p_n}}\right)\cos(\theta-\theta_n) - \eta_n w\sin(\theta-\theta_n)\right]\bar{u}_n = \bar{F}_n\cos\theta. \tag{34}$$

The combination of equations (32) and (34) gives the matrix formulation of charging on piezoelectric capacitance:

$$\tilde{\mathbf{Q}} = \tilde{\mathbf{C}}\tilde{\mathbf{V}}, \quad \tilde{\mathbf{Q}} = \left(\tilde{Q}_n\right), \quad \tilde{\mathbf{V}} = \left(\tilde{V}_n\right), \tag{35}$$

where

$$\tilde{Q}_n = \frac{C_{p_n}}{\Theta_n}\bar{F}_n, \quad \tilde{V}_n = \frac{\Theta_n}{C_{p_n}}\bar{u}_n e^{-j\theta_n}. \tag{36}$$

Above the capacitance matrix $\tilde{\mathbf{C}}$ is explicitly expressed as:

$$\tilde{C}_{kl} = \begin{cases} \left(\frac{C_{p_k}}{\Theta_k}\right)^2\left(K_k - w^2M_k + jw\eta_k\right) + C_{p_k} + \frac{1}{wZ_{\mathrm{eq}}^s} & \text{if } k = l, \\ \frac{1}{wZ_{\mathrm{eq}}^s} & \text{if } k \neq l, \end{cases} \tag{37}$$

with

$$Z_{\mathrm{eq}}^s = \frac{\pi}{4}\frac{1}{jwC_p^*}. \tag{38}$$

The harvested average power is given by:

$$P_h = \frac{\frac{1}{2}C_p^*V_M^2}{\frac{T}{2}}, \quad V_M = 2\left|\sum_{n=1}^{N}\tilde{V}_n\right|, \tag{39}$$

where the magnitude of piezoelectric voltage V_M of the present case is determined by equations (27), (29) and (36). Above each $\tilde{V}_n$ is the component of the generalized voltage vector $\tilde{\mathbf{V}}$ defined by equation (36). The determination of $\tilde{V}_n$ is thus achieved by inverting the matrix formulation of charging on capacitance as in equation (35).

3. Validation

The validation of the proposed SECE harvested power given by equation (22) for parallel connection and equation (39) for series connection of piezoelectric oscillators are carried out numerically through the conventional circuit simulation. Indeed, the governing equations of an array system provided by equations (1)–(3) can be explained from the circuit point of view. For example, a standard $R^*L^*C^*$ equivalent circuit model is introduced by assigning $R_n^* = \frac{\eta_n}{\Theta_n^2}$ as resistor, $L_n^* = \frac{M_n}{\Theta_n^2}$ as inductance, $C_n^* = \frac{\Theta_n^2}{K_n}$ as capacitance and $V_{\mathrm{source}}^n = \frac{\bar{F}_n}{\Theta_n}$ as voltage source [25, 36]. Now consider a case where four piezoelectric oscillators are connected in parallel (series) and is attached to an SECE interface. The associated equivalent circuit model for the harvester array is schematically depicted by figure 3(a) for the parallel connection and figure 3(b) for the series connection. The circuit simulation is performed using the SIMetrix mixed-mode circuit simulator offering enhanced SPICE (Simulation Program with Integrated Circuit Emphasis) (https://www.simetrix.co.uk).

The simulation results are presented by figure 4 where harvested power is shown against frequency evaluated at the load $R_L = 2\,\mathrm{M\Omega}$. The equivalent model parameters used in the simulations are given by table 1 which was obtained from the experiment presented in the next section. The prediction by the proposed framework is presented by the solid continuous blue line based on equation (22) for the case of parallel connection or equation (39) for the case of series connection. For the purpose of comparison, the electric losses are excluded in the simulations which are presented by various rectangle solid points of blue color. Clearly, figure 4 shows that the simulation results agree well with the analytic estimates for both arrangements of piezoelectric oscillators. Hence, it is concluded that the proposed analytic estimates are suitable for the performance evaluation of the electrical response of an SECE-based array of piezoelectric energy harvesters and therefore, provide a useful guidance for design analysis.

In addition, motivated by our experiment in section 4, the parallel and series connections of harvesters exhibited distinct levels of power reduction whose explanation can not be attributed to the common circuit losses discussed in appendix. Thus,

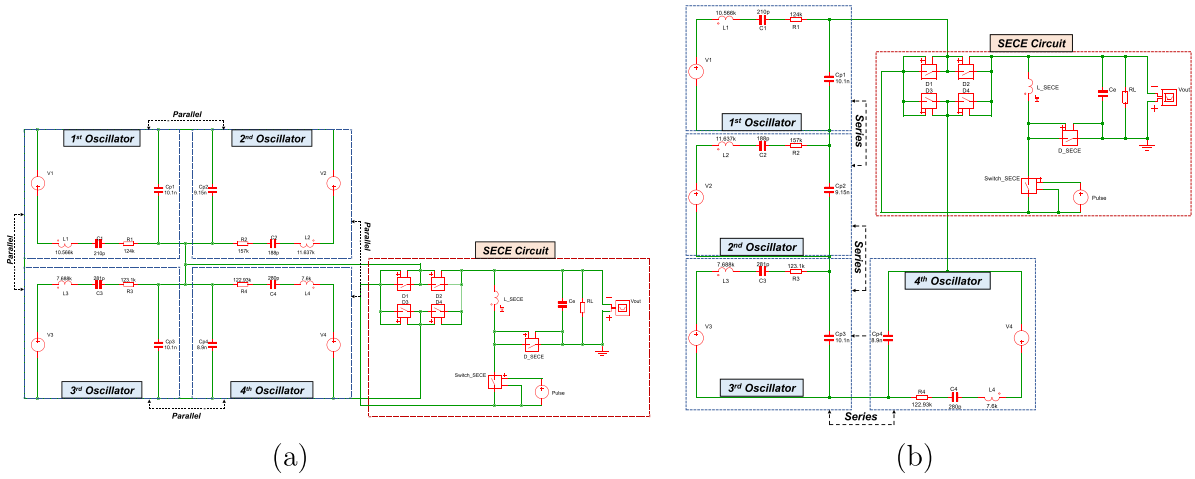

Figure 3. An equivalent circuit model for a device consisting of four piezoelectric oscillators attached to an SECE interface circuit: (a) parallel connection and(b) series connection.

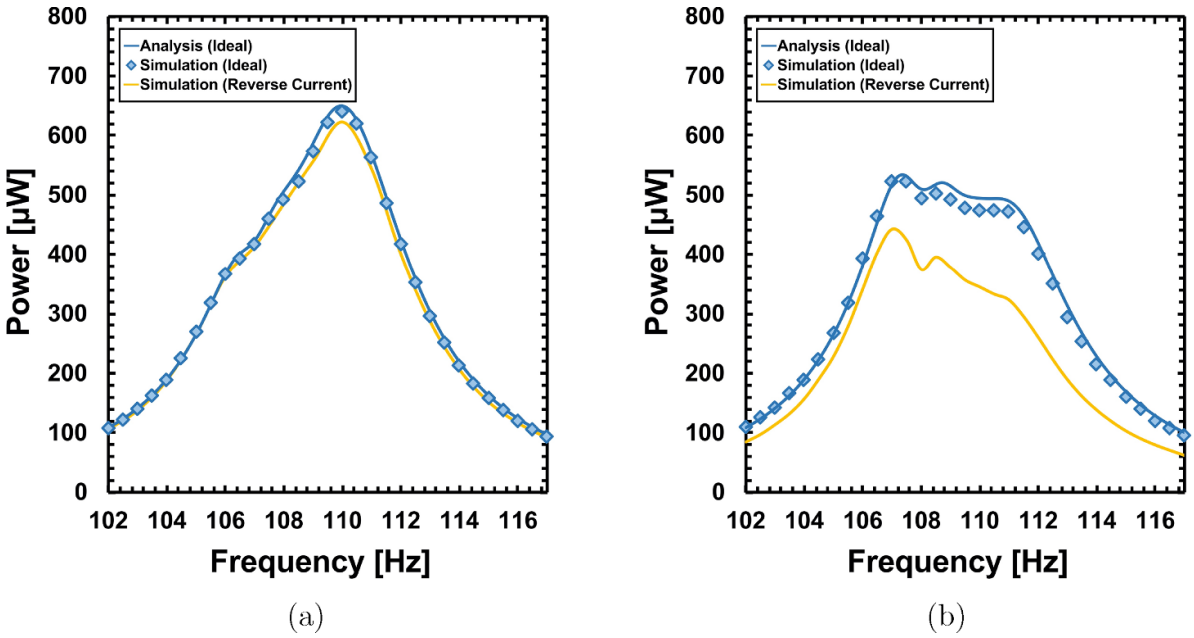

Figure 4. Numerical validation of the proposed analytic estimate of harvested power against frequency: (a) parallel connection and (b) series connection.

another circuit simulations are proposed for clarification. Consider the case where all forms of electric losses in the circuit elements are excluded except for the leakage current in the reversed-biased diodes. To simulate such a situation, the diode in figure 3 is modeled as a switch. It has an extremely small threshold voltage, a small on-resistance and a large off-resistance. In addition, 10 MΩ off-resistance is chosen for building a diode switch-model in the SIMetrix simulation. The harvested power considering only the effect of reverse current is presented by yellow color curves in figure 4. Clearly, figure 4(a) indicates a small deviation between the ideal case and the case accounting the leakage current in the array of oscillators connected in parallel. But a pronounced discrepancy is observed in the series connection of oscillators, as demonstrated in figure 4(b). These observations are consistent with those found in our recent experiment presented at the end of section 4.

4. Experiment

The experimental setup for validating the analytic model of an SECE array of piezoelectric oscillators is prepared and shown in figure 5(a). The device consists of 4 piezoelectric bimorphs manufactured by Eleceram Technology (Taiwan). They are clamped by a fixture mounted on the shaker (Data Physics, V20) operated by a signal generator through LabVIEW and a power amplifier (Data Physics, PA 300E). The accelerometer (PCB Piezotronics, 333B42) is placed on the top of the clamping fixture for measuring the acceleration of excitation from the shaker. Each cantilever bimorph contains

Table 1. The measured model parameters of the four piezoelectric cantilever bimorphs used in experiment.

	1st	2nd	3rd	4th
M (g)	1.654	1.655	1.764	1.804
K (kN m^{-1})	0.740	0.757	0.817	0.846
η (N s m^{-1})	0.019	0.022	0.028	0.029
Θ (mN V^{-1})	0.394	0.377	0.479	0.487
C_p (nF)	10.10	9.15	10.10	8.90
$\bar{F}$ (mN)	5.596	6.894	6.606	6.617
f_{sc} (Hz)	106.5	107.7	108.3	109.0
f_{oc} (Hz)	107.6	108.8	109.8	110.7
$\frac{k_e^2}{\zeta}$	2.39	2.05	2.42	2.67
R^{opt} (kΩ)	230	250	225	254
P^{opt} (μW)	162	197	158	157

two PZT layers on the top and the bottom with $70 \times 10 \times 0.3$ mm^3 in dimensions. The central substrate layer is made of Cu with $70 \times 10 \times 0.5$ mm^3 in dimensions. The resonant frequency of each cantilever bimorph is tuned by various magnitudes of proof mass bounded to its free end. The equivalent parameters of each cantilever bimorph are identified by the conventional modal testing [76] and are listed in table 1. In the table, the short circuit and open circuit resonant frequencies of each oscillator are denoted by f_{sc} and f_{oc}, respectively. In addition, R^{opt} is the electric load for generating the optimal power output P^{opt}.

The SECE circuit is attached to the piezoelectric array arranged electrically either in parallel (1//2//3//4) or series (1+2+3+4) connection. Its switch element is made of N-MOSFET which is controlled by the pulse of the function generator. The pulse width (PW) is set according to the value $\pi\sqrt{C_p^* L_{SECE}}/2$ where the magnitude of the inductor L_{SECE} here is about 100 mH for increasing the inversion factor [77]. In addition, the pulse frequency is chosen to be the twice of the excitation frequency. Its phase is adjusted to match the instant of the peak of piezoelectric voltage, giving rise to the inversion of the piezoelectric voltage V_p whose measured waveform is illustrated in figure 5(b). During the operation, the output DC voltage across the electric load is measured and recorded through the DAQ device (NI 9178 and NI 9229). As the proposed analysis does not account for the losses in various electric elements, the comparison between the prediction and experiment requires the measurement of these losses. These include the conversion efficiency between the energy stored in piezoelectric capacitor and that partially transferred to the inductor, and the power dissipations due to voltage drops in the full-bridge rectifier and the flyback diode in the converter, respectively. The formulations of estimating these various electric losses are presented in appendix.

The harvester array is excited under 0.15 g by a sine sweep signal over the frequency range of 100–120 Hz through a vibration shaker. Besides the SECE circuit, the standard (STD) interface circuit is also adopted for performance comparison. Note that the theoretical prediction of harvested power of an STD array can be found in the work by Lien and Shu [36] (parallel connection) and Lin *et al* [47] (series connection). Figure 6(a) shows the harvested power against frequency for the parallel connection of oscillators attached to either the SECE (blue color) or the STD (red color) interface circuit. The analytic estimate is presented by continuous color line while the experimental measurements are marked by solid color points. The electric load for the STD array is chosen to be 73 kΩ (optimal for harvested power) and is chosen to be 2 MΩ for the SECE array. Note that the variations of load resistance on the output SECE power will be discussed later. From figure 6(a), the harvested power achieved by the SECE array is clearly higher than that by the STD array. Precisely, the ratio of peak power of the SECE array to that of the STD array is 156% based on the ideal analysis and is 157% from the experiment. Such a result is consistent with that based on a single piezoelectric oscillator. Indeed, let the alternative electromechanical coupling k_e^2 and the mechanical damping ratio ζ be defined by:

$$k_e^2 = \frac{\Theta^2}{KC_p}, \quad \zeta = \frac{\eta}{2\sqrt{KM}}.$$

It has been shown that the SECE power achieves the maximal value and outperforms the STD power if the ratio $\frac{k_e^2}{\zeta} = \frac{\pi}{2}$ for the case of a single piezoelectric harvester [78]. While the optimal ratio of this indicator is unknown for the array configuration, table 1 lists this ratio for each cantilever bimorph and shows its range is from 2.05 to 2.67 whose values are not far from $\frac{\pi}{2}$. Thus, it confirms the superiority of the use of SECE interface in the case of mild electromechanical coupling. Finally, as the analysis presented in section 2 is based on the loss-free condition, figure 6(b) shows that comparison between the prediction and the experiment compensated with power dissipations on switching and diode losses (see the discussion in appendix). Clearly, good agreement is found and it confirms the proposed estimate of power is suitable for the performance evaluation of the electrical behavior of an SECE array with parallel connection of oscillators.

Next, consider the case of piezoelectric oscillators electrically connected in series. Figure 7(a) shows harvested power against frequency for the series connection of piezoelectric oscillators attached to either the SECE (blue color) or the STD (red color) interface circuit. Similar to the previous case of parallel connection, harvested power based on the SECE circuit is much larger than that based on the STD interface. The ratio of peak power of the SECE array to the STD array is 138% based on the ideal analysis and is 137% for the experiment. In addition, the bandwidth of the former is clearly much wider than the latter, as illustrated in figure 7(a). But different from the previous case shown in figure 6(a), the series connection of the SECE array exhibits much more uniform in power frequency response than that presented by the parallel connection of the SECE array at the cost of peak magnitude of output power.

In addition, figure 7(b) compares the prediction to the experiment compensated with power dissipations on switching and diode losses based on the estimates proposed in appendix [79]. It is found that there is a significant discrepancy between these two. Such a phenomenon is very different from

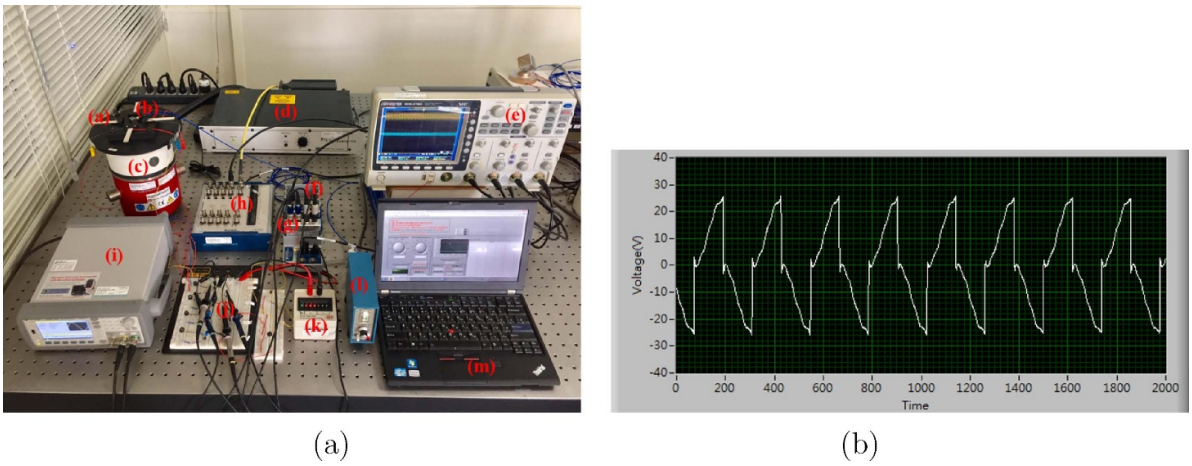

(a) (b)

Figure 5. The LHS is the experimental setup: (a) is the array consisting of 4 piezoelectric bimorphs clamped on a fixture, (b) accelerometer, (c) shaker, (d) power amplifier, (e) oscilloscope, (f)–(h) NI DAQ sets, (i) signal generator, (j) SECE interface circuit, (k) resistance substitution box, (l) signal conditioner for accelerometer (m) computer installed with LabVIEW. The RHS is the waveform of the piezoelectric voltage under the SECE operation.

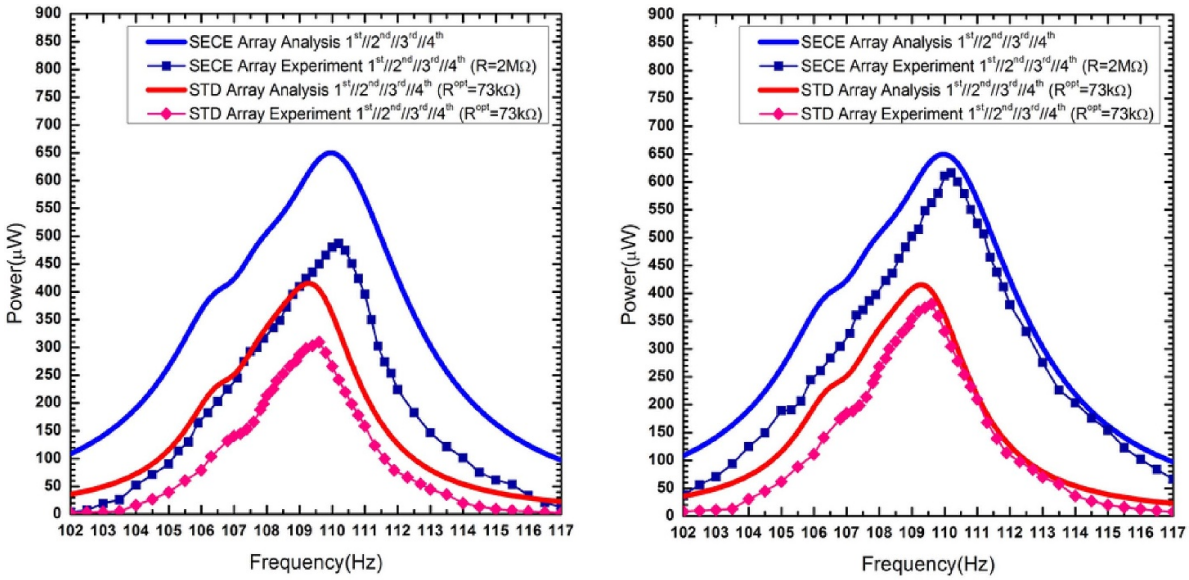

(a) (b)

Figure 6. Harvested power against frequency for the SECE (blue) and STD (red) array of four piezoelectric harvesters electrically arranged in parallel connection. The analytic prediction (the experiment) is presented by the continuous curve (solid points). Note that the experimental observations shown in (a) are original data, while those shown in (b) include the power dissipated at diodes and switching process.

the previous case shown in figure 6(b). We seek explanations and found the observed incongruity might be explained as the effect of the reverse current flowing through the reverse-biased diodes. Indeed, the operation of ideal full bridge rectifier converts the alternating signal into the same polarity, keeping the conduct of current in only one pair of diodes and leaving the other pair inactive at the same instant of time. But in reality there exists a small amount of leakage current in the reverse-biased diodes, and the magnitude of it is proportional to that of the piezoelectric voltage. As a result, power loss is more pronounced in the series connection of oscillators than that arranged in the parallel connection since the former typically exhibits larger voltage than the latter. To support this idea, the yellow curves in figure 4 are the simulation results accounting only for the effect of reverse current and excluding other electric losses. Obviously, the experiments shown in figure 6(b) (parallel connection) and figure 7(b) (series connection) exhibit the similar trend as simulated in figure 4. Thus, the conjecture of leakage current in the reverse-biased diodes might be the main reason explaining the significant power drop in the series connection of multiple piezoelectric oscillators.

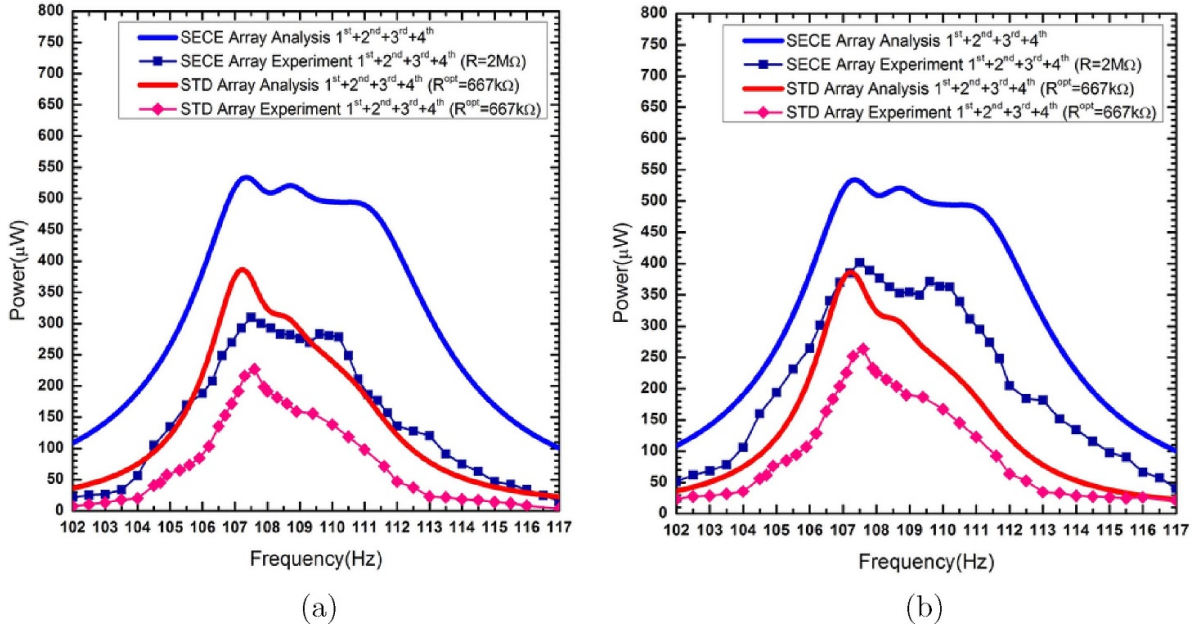

Figure 7. Harvested power against frequency for the SECE (blue) and STD (red) array of four piezoelectric harvesters electrically arranged in series connection. The analytic prediction (the experiment) is presented by the continuous curve (solid points). Note that the experimental observations shown in (a) are original data, while those shown in (b) include the power dissipated at diodes and switching process.

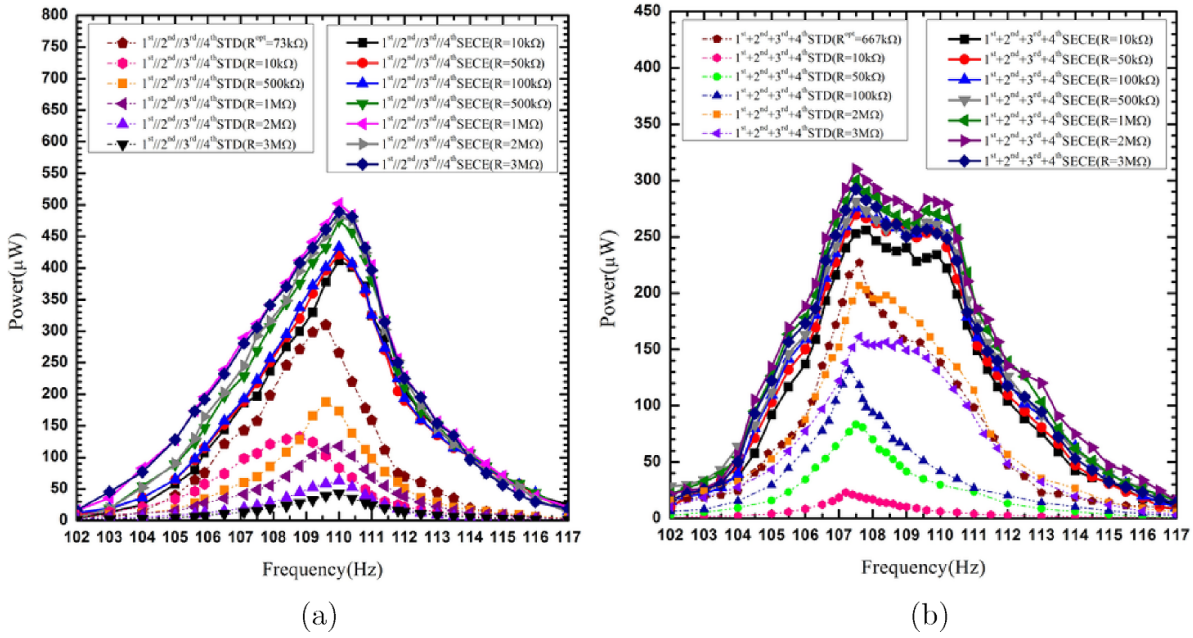

Figure 8. Harvested power against frequency evaluated under various electric loads for the SECE (continuous lines) and STD (dashed lines) arrays: (a) parallel connection of harvesters and (b) series connection of harvesters.

The effect of electric load on harvested power against frequency is discussed and presented in figure 8(a) for the parallel connection and figure 8(b) for the series connection. For electric loads chosen from 10 kΩ to 3 MΩ, it is found that the output power of the SECE array exhibits the load-insensitive property as demonstrated in figure 8. Indeed, the peak power ranges from 412 to 501 μW for the parallel connection and from 256 to 310 μW for the series connection, as illustrated by table 2. Notice that the variations of the SECE harvested power along with the electric load are mainly attributed to power dissipations on flyback diode losses which are increased as the decrease of electric loads according to appendix. In addition, table 2 also lists the DC voltage across the load and the current passing through the load for comparison. As the regular sensor nodes are typically operated at around 2–5 V, in this range, table 2 shows that the generated current can be up to 200 μA in the case of SECE array arranged electrically in parallel.

Table 2. The peaks of harvested power evaluated at various electric loads for the SECE array arranged electrically in parallel and series. The corresponding DC voltage across the load and the current passing through the load are also listed for comparison.

Electric load	10 kΩ	50 kΩ	100 kΩ	500 kΩ	1 MΩ	2 MΩ	3 MΩ	Ave power
$P^{\mathrm{SECE}}_{\mathrm{parallel}}$ (μW)	412.1	421.4	433.0	474.3	501.8	486.9	489.0	460.0
$V^{\mathrm{SECE}}_{\mathrm{parallel}}$ (V)	2.0	4.6	6.6	15.4	22.4	31.2	38.2	
$I^{\mathrm{SECE}}_{\mathrm{parallel}}$ (μA)	203.0	91.8	65.8	30.8	22.4	15.6	12.8	
Electric load	10 kΩ	50 kΩ	100 kΩ	500 kΩ	1 MΩ	2 MΩ	3 MΩ	Ave power
$P^{\mathrm{SECE}}_{\mathrm{series}}$ (μW)	256.0	269.3	275.6	281.3	300.3	310.0	292.3	283.5
$V^{\mathrm{SECE}}_{\mathrm{series}}$ (V)	1.6	3.7	5.2	11.9	17.3	25.0	29.5	
$I^{\mathrm{SECE}}_{\mathrm{series}}$ (μA)	160.0	73.4	52.5	23.7	17.3	12.4	9.9	

Table 3. The peaks of harvested power evaluated at various electric loads for the STD array arranged electrically in parallel and series. The corresponding DC voltage across the load and the current passing through the load are also listed for comparison.

Electric load	10 kΩ	73 kΩ	500 kΩ	1 MΩ	2 MΩ	3 MΩ	Ave power
$P^{\mathrm{STD}}_{\mathrm{parallel}}$ (μW)	132.4	309.8	187.8	117.8	63.1	43.3	142.4
$V^{\mathrm{STD}}_{\mathrm{parallel}}$ (V)	1.15	4.8	9.7	10.9	11.3	11.4	
$I^{\mathrm{STD}}_{\mathrm{parallel}}$ (μA)	115.0	65.1	19.4	10.9	5.6	3.8	
Electric load	10 kΩ	50 kΩ	100 kΩ	667 kΩ	2 MΩ	3 MΩ	Ave power
$P^{\mathrm{STD}}_{\mathrm{series}}$ (μW)	23.0	83.2	131.8	227.0	206.7	161.2	138.8
$V^{\mathrm{STD}}_{\mathrm{series}}$ (V)	0.5	2.0	3.6	12.3	20.3	22.1	
$I^{\mathrm{STD}}_{\mathrm{series}}$ (μA)	48.0	40.8	36.3	18.4	10.2	7.3	

Finally, figure 8 also indicates the significant sensitivity of power against loads for the STD array. Specifically, for electric loads chosen from 10 kΩ to 3 MΩ, the peak power ranges from 43 to 309 μW for the parallel connection while it ranges from 23 to 227 μW for the series connection, as indicated in table 3. In addition, a further examination of table 3 reveals the arrangement of the parallel connection provides the significant increase of output current in comparison with the series connection of harvesters [80]. Indeed, table 3 indicates the optimal output power is 309.8 μW evaluated at 73 kΩ in the case of parallel connection. This gives the DC voltage 4.8 V and current 65.1 μA. In comparison to the case of the series connection, the optimal harvested power is 227 μW evaluated at 667 kΩ, giving rise to the DC voltage 12.3 V and current 18.4 μA.

5. Conclusions

The paper examines the electrical behavior of multiple piezoelectric energy harvesters connected to an SECE interface circuit. The harvested power is analytically derived and explicitly presented through the matrix formulation of generalized Ohms's law (charging on capacitance) for the case of parallel (series) connection of oscillators, as in equations (19) and (35). Notice that the generalized impedance matrix $\hat{\mathbf{Z}}$ as in equation (20) as well as the generalized capacitance matrix $\tilde{\mathbf{C}}$ as in equation (37) are explicitly expressed in terms of the system parameters and the equivalent load impedance Z^p_{eq} or Z^s_{eq}. Interestingly, both Z^p_{eq} and Z^s_{eq} are found to be independent of external loads, so is harvested power.

The proposed estimate of output power is numerically validated through the conventional circuit simulation. The prediction is found in good agreement with the simulation. It is also experimentally validated by a setup consisting of four piezoelectric oscillators. Several observations drawn from experiment are listed here. First, it is found that both the power output and bandwidth of an array based on the SECE interface is much better than that based on the standard interface in the medium range of electromechanical coupling. Second, the electrical response of an SECE array arranged in parallel connection is different from that connected in series. The output power of the former is higher than the latter, while the latter has roughly uniform peak power in frequency response. However, in contrast to the case of parallel connection, the harvested power of an array connected in series is experimentally observed to be much smaller than the theoretical prediction. The discrepancy found in the series case is explained as a result of relatively severe leakage current in the reverse-biased diodes.

Acknowledgments

The authors are glad to acknowledge the support from Ministry of Science and Technology under Grant Nos. 105-2221-E-002-028-MY3 and 108-2221-E-002-004-MY3.

Appendix. Various electric losses in the SECE power conditioning process

On the basis of ideal rectification and complete energy transfer from the piezoelectric capacitance to the inductor, the estimate of output power from the SECE-based array was developed

in section 2. But electric losses are inevitable in the practical power conditioning process. Thus, it is essential to realize the power dissipations in various electric elements for fair comparison between the prediction and experiment. This issue was studied by Chen *et al* [79] who concluded three paths causing the energy dissipations. Indeed, let ΔV_{bridge} be the forward voltage drop in the bridge rectifier, γ be the ratio of energy stored in the inductor L_{SECE} to that stored in the overall piezoelectric capacitance C_p^*, and $\Delta V_{\text{flyback}}$ be the voltage drop in the flyback diode. The total power dissipations in a half cycle vibration $\frac{T}{2} = \frac{\pi}{w}$ during the SECE energy extraction process are:

$$P_{\text{d, tot}} = P_{\text{d, bridge}} + P_{\text{d,switch}} + P_{\text{d, flyback}}, \tag{A1}$$

where

$$P_{\text{d, bridge}} = \frac{C_p^* \Delta V_{\text{bridge}} V_M}{T/2}, \tag{A2}$$

$$P_{\text{d, switch}} = \frac{\frac{1}{2}(1-\gamma) C_p^* V_M (V_M - 2\Delta V_{\text{bridge}})}{T/2}, \tag{A3}$$

$$P_{\text{d, flyback}} = \Delta V_{\text{flyback}} \times \frac{V_c}{R_L}. \tag{A4}$$

Above recall V_M is the twice of the open circuit voltage, V_c is the DC voltage across the external load R_L, and

$$\gamma = \frac{\frac{1}{2} L_{\text{SECE}} i_L^2}{\frac{1}{2} C_p^* V_M^2 - C_p^* \Delta V_{\text{bridge}} V_M}, \tag{A5}$$

where i_L is the current passing through the inductor L_{SECE}. Practically, it is obtained by measuring the voltage drop of a small resistance attached to the ends of the inductor. In addition, ΔV_{bridge} and $\Delta V_{\text{flyback}}$ can be measured in experiment for estimating power dissipations in the bridge rectifier and flyback diode. Note that $\gamma = 0.83$ was observed by Chen *et al* [79] for the case of a single harvester. In the present case of harvester array, γ was measured around 0.8 for the parallel connection and was around 0.6 for the series connection of harvesters.

ORCID iD

Y C Shu https://orcid.org/0000-0003-3842-8128

References

[1] Erturk A and Inman D J 2011 *Piezoelectric Energy Harvesting* (New York: Wiley)

[2] Le C P, Halvorsen E, Søråsen O and Yeatman E M 2013 Wideband excitation of an electrostatic vibration energy harvester with power-extracting end-stops *Smart Mater. Struct.* **22** 075020

[3] Thein C K, Foong F M and Shu Y C 2019 Spring amplification and dynamic friction modelling of a 2DOF/2SDOF system in an electromagnetic vibration energy harvester—experiment, simulation and analytical analysis *J. Mech. Syst. Signal Process.* **132** 232–52

[4] Roundy S, Wright P K and Rabaey J 2003 A study of low level vibrations as power source for wireless sensor nodes *Comput. Commun.* **26** 1131–44

[5] Aktakka E E and Najafi K 2014 A micro inertial energy harvesting platform with self-supplied power management circuit for autonomous wireless sensor nodes *IEEE J. Solid-State Circuits* **49** 2017–29

[6] Shu Y C and Lien I C 2006 Efficiency of energy conversion for a piezoelectric power harvesting system *J. Micromech. Microeng.* **16** 2429–38

[7] Bayik B, Aghakhani A, Basdogan I and Erturk A 2016 Equivalent circuit modeling of a piezo-patch energy harvester on a thin plate with AC–DC conversion *Smart Mater. Struct.* **25** 055015

[8] Liao Y and Sodano H 2018 Optimal power, power limit and damping of vibration based piezoelectric power harvesters *Smart Mater. Struct.* **27** 075057

[9] Lumentut M F and Shu Y C 2020 Shunted optimal vibration energy harvesting control of discontinuous smart beams *Compos. Struct.* **242** 112126

[10] Lumentut M F and Shu Y C 2021 Network segmentations of smart plate structure with attached mass and dynamic motions *Eur. J. Mech.* A **85** 104061

[11] Pozzi M 2016 Magnetic plucking of piezoelectric bimorphs for a wearable energy harvester *Smart Mater. Struct.* **25** 045008

[12] Qian F, Zhou W, Kaluvan S, Zhang H and Zuo L 2018 Theoretical modeling and experimental validation of a torsional piezoelectric vibration energy harvesting system *Smart Mater. Struct.* **27** 045018

[13] Yan X, Zheng M, Zhu M and Hou Y 2020 Soft and hard piezoelectric ceramics for vibration energy harvesting *Crystals* **10** 907

[14] Badel A, Benayad A, Lefeuvre E, Lebrun L, Richard C and Guyomar D 2006 Single crystals and nonlinear process for outstanding vibration-powered electrical generators *IEEE Trans. Ultrason. Ferroelectr. Freq. Control* **53** 673–84

[15] Guyomar D, Badel A, Lefeuvre E and Richard C 2005 Toward energy harvesting using active materials and conversion improvement by nonlinear processing *IEEE Trans. Ultrason. Ferroelectr. Freq. Control* **52** 584–95

[16] Hsieh P H, Chen C H and Chen H C 2015 Improving the scavenged power of nonlinear piezoelectric energy harvesting interface at off-resonance by introducing switching delay *IEEE Trans. Power Electron.* **30** 3142–55

[17] Lallart M and Guyomar D 2008 An optimized self-powered switching circuit for non-linear energy harvesting with low voltage output *Smart Mater. Struct.* **17** 035030

[18] Lien I C, Shu Y C, Wu W J, Shiu S M and Lin H C 2010 Revisit of series-SSHI with comparisons to other interfacing circuits in piezoelectric energy harvesting *Smart Mater. Struct.* **19** 125009

[19] Shu Y C and Lien I C 2006 Analysis of power output for piezoelectric energy harvesting systems *Smart Mater. Struct.* **15** 1499–512

[20] Shu Y C, Lien I C and Wu W J 2007 An improved analysis of the SSHI interface in piezoelectric energy harvesting *Smart Mater. Struct.* **16** 2253–64

[21] Gedeon D and Rupitsch S J 2018 Finite element based system simulation for piezoelectric vibration energy harvesting devices *J. Intell. Mater. Syst. Struct.* **29** 1333–47

[22] Lumentut M F and Shu Y C 2018 A unified electromechanical finite element dynamic analysis of multiple segmented smart plate energy harvesters: circuit connection patterns *Acta Mech.* **229** 4575–604

[23] Thein C K, Foong F M and Shu Y C 2019 Damping ratio and power output prediction of an electromagnetic energy harvester designed through finite element analysis *Sensors Actuators* A **286** 220–31

[24] Wu P H and Shu Y C 2015 Finite element modeling of electrically rectified piezoelectric energy harvesters *Smart Mater. Struct.* **24** 094008

[25] Yang Y and Tang L 2009 Equivalent circuit modeling of piezoelectric energy harvesters *J. Intell. Mater. Syst. Struct.* **20** 2223–35

[26] Ansari M H and Karami M A 2017 Experimental investigation of fan-folded piezoelectric energy harvesters for powering pacemakers *Smart Mater. Struct.* **26** 065001

[27] Lallart M, Anton S R and Inman D J 2010 Frequency self-tuning scheme for broadband vibration energy harvesting *J. Intell. Mater. Syst. Struct.* **21** 897–906

[28] Kamali S H, Moallem M and Arzanpour S 2018 A self-tuning vibration energy harvester with variable loads and maximum allowable displacement *Smart Mater. Struct.* **27** 105015

[29] Erturk A, Hoffmann J and Inman D J 2009 A piezomagnetoelastic structure for broadband vibration energy harvesting *Appl. Phys. Lett.* **94** 254102

[30] Upadrashta D and Yang Y 2016 Nonlinear piezomagnetoelastic harvester array for broadband energy harvesting *J. Appl. Phys.* **120** 054504

[31] Zhang C, Harne R L, Li B and Wang K W 2020 Harmonic analysis and experimental validation of bistable vibration energy harvesters interfaced with rectifying electrical circuits *Commun. Nonlinear Sci. Numer. Simul.* **82** 105069

[32] Fu H and Yeatman E M 2017 A methodology for low-speed broadband rotational energy harvesting using piezoelectric transduction and frequency up-conversion *Energy* **125** 152–61

[33] Shu Y C, Wang W C and Chang Y P 2018 Electrically rectified piezoelectric energy harvesting induced by rotary magnetic plucking *Smart Mater. Struct.* **27** 125006

[34] Xue T and Roundy S 2017 On magnetic plucking configurations for frequency up-converting mechanical energy harvesters *Sensors Actuators* A **253** 101–11

[35] Dechant E, Fedulov F, Fetisov L Y and Shamonin M 2017 Bandwidth widening of piezoelectric cantilever beam arrays by mass-tip tuning for low-frequency vibration energy harvesting *Appl. Sci.* **7** 1324

[36] Lien I C and Shu Y C 2012 Array of piezoelectric energy harvesting by equivalent impedance approach *Smart Mater. Struct.* **21** 082001

[37] Lumentut M F, Francis L A and Howard I M 2012 Analytical techniques for broadband multielectromechanical piezoelectric bimorph beams with multifrequency power harvesting *IEEE Trans. Ultrason. Ferroelectr. Freq. Control* **59** 2555–68

[38] Abramovich H and Har-nes I 2018 Analysis and experimental validation of a piezoelectric harvester with enhanced frequency bandwidth *Materials* **11** 1243

[39] Baú M, AlghisiIand D Dalola S, Ferrari M and Ferrari V 2020 Multi-frequency array of nonlinear piezoelectric converters for vibration energy harvesting *Smart Mater. Struct.* **29** 085047

[40] Ma T, Chen N, Wu X, Du F and Ding Y 2019 Investigation on the design and application of 3-dimensional wide-band piezoelectric energy harvester for low amplitude vibration sources *Smart Mater. Struct.* **28** 105013

[41] Kuang Y and Zhu M 2016 Characterisation of a knee-joint energy harvester powering a wireless communication sensing node *Smart Mater. Struct.* **25** 055013

[42] Xiao Z, Yang T Q, Dong Y and Wang X C 2014 Energy harvester array using piezoelectric circular diaphragm for broadband vibration *Appl. Phys. Lett.* **104** 223904

[43] Shi Q, Wang T and Lee C 2016 MEMS based broadband piezoelectric ultrasonic energy harvester (PUEH) for enabling self-powered implantable biomedical devices *Sci. Rep.* **6** 24946

[44] Lien I C and Shu Y C 2011 Array of piezoelectric energy harvesters *Proc. SPIE* **7977** 215–23

[45] Xia H and Chen R 2014 Design and analysis of a scalable harvesting interface for multi-source piezoelectric energy harvesting *Sensors Actuators* A **218** 33–40

[46] Zhang Y, Bian K, Gu Y, Ye M, Tian W and Liu W 2020 Cost-effective and scalable rectifier design for multiple piezoelectric power sources with improved performance *J. Intell. Mater. Syst. Struct.* **31** 167–81

[47] Lin H C, Wu P H, Lien I C and Shu Y C 2013 Analysis of an array of piezoelectric energy harvesters connected in series *Smart Mater. Struct.* **22** 094026

[48] Wu P H, Chen Y J, Li B Y and Shu Y C 2017 Wideband energy harvesting based on mixed connection of piezoelectric oscillators *Smart Mater. Struct.* **26** 094005

[49] Tang L and Yang Y 2011 Analysis of synchronized charge extraction for piezoelectric energy harvesting *Smart Mater. Struct.* **20** 085022

[50] Lefeuvre E, Badel A, Richard C and Guyomar D 2007 Energy harvesting using piezoelectric materials: case of random vibrations *J. Electroceram.* **19** 349–55

[51] Lefeuvre E, Badel A, Richard C and Guyomar D 2005 Piezoelectric energy harvesting device optimization by synchronous electric charge extraction *J. Intell. Mater. Syst. Struct.* **16** 865–76

[52] Wu Y, Badel A, Formosa F, Liu W and Agbossou A E 2013 Piezoelectric vibration energy harvesting by optimized synchronous electric charge extraction *J. Intell. Mater. Syst. Struct.* **24** 1445–58

[53] Wu Y, Badel A, Formosa F, Liu W and Agbossou A E 2014 Self-powered optimized synchronous electric charge extraction circuit for piezoelectric energy harvesting *J. Intell. Mater. Syst. Struct.* **25** 2165–76

[54] Lefeuvre E, Badel A, Brenes A, Seok S, Woytasik M and Yoo C S 2017 Analysis of piezoelectric energy harvesting system with tunable SECE interface *Smart Mater. Struct.* **26** 035065

[55] Morel A, Quelen A, Gasnier P, Grezaud R, Monfray S, Badel A and Pillonnet G 2018 A unified N-SECE strategy for highly coupled piezoelectric energy scavengers *Smart Mater. Struct.* **27** 084002

[56] Xia H, Xia Y, Ye Y, Qian L, Shi G and Chen R 2018 Analysis and simulation of synchronous electric charge partial extraction technique for efficient piezoelectric energy harvesting *IEEE Sens. J.* **18** 6235–44

[57] Lefeuvre E, Badel A, Brenes A, Seok S and Yoo C S 2017 Power and frequency bandwidth improvement of piezoelectric energy harvesting devices using phase-shifted synchronous electric charge extraction interface circuit *J. Intell. Mater. Syst. Struct.* **28** 2988–95

[58] Brenes A, Morel A, Gibus D, Yoo C S, Gasnier P, Lefeuvre E and Badel A 2020 Large-bandwidth piezoelectric energy harvesting with frequency-tuning synchronized electric charge extraction *Sens. Actuator A Phys.* **302** 111759

[59] Liu W, Zhao C, Badel A, Formoas F, Zhu Q and Hu G 2018 Compact self-powered synchronous energy extraction circuit design with enhanced performance *Smart Mater. Struct.* **27** 047001

[60] Liu W, Badel A, Formosa F, Zhu Q, Zhao C and Hu G D 2018 A comprehensive analysis and modeling of the self-powered synchronous switching harvesting circuit with electronic breakers *IEEE Trans. Ind. Electron.* **65** 3899–909

[61] Shi G, Xia Y, Ye Y, Qian L and Li Q 2016 An Efficient self-powered synchronous electric charge extraction interface circuit for piezoelectric energy harvesting systems *J. Intell. Mater. Syst. Struct.* **27** 2160–78

[62] Lallart M, Wu W J, Hsieh Y and Yan L 2017 Synchronous inversion and charge extraction (SICE): a hybrid switching interface for efficient vibrational energy harvesting *Smart Mater. Struct.* **26** 115012
[63] Shen H, Qiu J, Ji H, Zhu K and Balsi M 2010 Enhanced synchronized switch harvesting: a new energy harvesting scheme for efficient energy extraction *Smart Mater. Struct.* **19** 115017
[64] Xia H, Xia Y, Shi G, Ye Y, Wang X, Chen Z and Jiang Q 2020 A self-powered S-SSHI and SECE hybrid rectifier for PE energy harvesters: analysis and experiment *IEEE Trans. Power Electron.* **36** 1680–92
[65] Huguet T, Lallart M and Badel A 2019 Bistable vibration energy harvester and SECE circuit: exploring their mutual influence *Nonlinear Dyn.* **97** 485–501
[66] Li Z, Xiong L, Tang L, Liu K and Mace B 2020 Vibration energy harvesting based on a piezoelectric nonlinear energy sink with synchronized charge extraction interface circuit *J. Phys. D: Appl. Phys.* **53** 505502
[67] Liu W Q, Badel A, Formosa F, Wu Y P and Agbossou A 2013 Wideband energy harvesting using a combination of an optimized synchronous electric charge extraction circuit and a bistable harvester *Smart Mater. Struct.* **22** 125038
[68] Romani A, Filippi M and Tartagni M 2014 Micropower design of a fully autonomous energy harvesting circuit for arrays of piezoelectric transducers *IEEE Trans. Power Electron.* **29** 729–39
[69] Shareef A, Goh W L, Narasimalu S and Gao Y 2019 A rectifier-less AC-DC interface circuit for ambient energy harvesting from low-voltage piezoelectric transducer array *IEEE Trans. Power Electron.* **34** 1446–57
[70] Wang X, Xia Y, Du Y, Xia H, Shi G, Ye Y and Chen Z 2021 Multi-input SECE based on buck structure for piezoelectric energy harvesting *IEEE Trans. Power Electron.* **36** 3638–42
[71] Wang X, Xia Y, Shi G, Xia H, Ye Y and Chen Z 2020 Self-powered piezoelectric and thermoelectric energy simultaneous extraction interface circuit based on double stack resonance *IEEE Trans. Ind. Electron.* **67** 4567–77
[72] Zhao L, Tang L, Liang J and Yang Y 2017 Synergy of wind energy harvesting and synchronized switch harvesting interface circuit *IEEE/ASME Trans. Mechatronics* **22** 1093–103
[73] Boisseau S, Gasnier P, Perez M, Bouvard C, Geisler M, Duret A B, Despesse G and Willemin J 2015 Synchronous electric charge extraction for multiple piezoelectric energy harvesters *IEEE 13th Int. New Circuits and Systems Conf.* pp 1–4
[74] Lo Y C, Huang P H and Shu Y C 2020 Self-powered SECE-based piezoelectric energy harvesting for sensor supply under shock excitations *Proc. SPIE* **11376** 1137609
[75] Wu P H and Shu Y C 2015 Wideband energy harvesting by multiple piezoelectric oscillators with an sece interface *Proc. ASME 2015th Conf. Smart Materials, Adaptive Structures and Intelligent Systems* (SMASIS) pp 2015–8862
[76] Lin J T 2019 The experimental study of an array of piezoelectric energy oscillators attached to the synchronized electric charge extraction interface circuit MS Thesis National Taiwan University (https://doi.org/10.6342/NTU201902356)
[77] Liu J Chen Z, He J and Xiong Y 2019 Switching delay in self-powered nonlinear piezoelectric vibration energy harvesting circuit: mechanisms, effects *IEEE Trans. Power Electron.* **34** 2427–40
[78] Lefeuvre E, Badel A, Richard C, Petit L and Guyomar D 2006 A Comparison between several vibration-powered piezoelectric generators for standalone systems *Sensors Actuators* A **126** 405–16
[79] Chen C, Zhao B and Liang J 2019 Revisit of synchronized electric charge extraction (SECE) in piezoelectric energy harvesting by using impedance modeling *Smart Mater. Struct.* **28** 105053
[80] Woo M S, Baek K H, Kim J H, Kim S B, Song D and Sung T H 2015 Relationship between current and impedance in piezoelectric energy harvesting system for water waves *J. Electroceram.* **34** 180–4